Measurement of regional myocardial blood flow using $C^{15}O_2$ and positron emission tomography: comparison of tracer models

Clin. Phys. Physiol. Meas., 1992, Vol. 13, No. 1, 1–20. Printed in the UK

Measurement of regional myocardial blood flow using $C^{15}O_2$ and positron emission tomography: comparison of tracer models

Adriaan A Lammertsma, Ranil De Silva, Luis I Araujo and Terry Jones
MRC Cyclotron Unit, Hammersmith Hospital, London, UK

Received 23 April 1991, in final form 14 August 1991

Abstract. Eight different modifications of the same single tissue compartment model to measure myocardial blood flow, based on inhalation of ^{15}O-labelled CO_2 and positron emission tomography, were assessed in both dogs and human normal volunteers. Several models provided results with the same degree of accuracy in dogs. However, a number of these models gave poorer results in humans. It was established that the model containing components for blood flow, fraction of water exchanging tissue and spill-over arterial blood volume provided the most accurate and reproducible results. This model contains inherent corrections for the limited spatial resolution of positron emission tomographs. For ease of computation, linearisation of the operational (fitting) equation was tested, but found not to be satisfactory. The left atrium was slightly better than the left ventricle for determining the arterial input function. Inclusion of the blood volume term in the fitting procedure was significantly better than subtracting blood volume prior to analysis, both in terms of accuracy and precision.

1. Introduction

Myocardial blood flow (MBF) is an important parameter in the assessment of myocardial ischaemia, infarction and other pathological conditions where angiographic data are inconclusive. Using positron emission tomography (PET) several tracer procedures have been proposed for non-invasive regional MBF measurements, based on the following three radiotracers: $^{13}NH_3$ (Schelbert *et al* 1979, 1981, Krivokapich *et al* 1989, Bellina *et al* 1990, Hutchins *et al* 1990), ^{82}Rb (Budinger *et al* 1980, Selwyn *et al* 1982, Mullani *et al* 1983, Huang *et al* 1989, Herrero *et al* 1990) and $H_2{}^{15}O$ (Bergmann *et al* 1984, 1989, Huang *et al* 1985, Iida *et al* 1988). Of these three tracers $H_2{}^{15}O$ has the advantage that (in the myocardium) it is freely diffusible (Johnson *et al* 1952, Yipintsoi and Bassingthwaite 1970) and metabolically inert (Bergmann *et al* 1984). This implies that it can be used reliably in metabolically impaired myocardium. In addition, the short half-life of oxygen-15 is an important advantage if repeat measurements are required (e.g. following pharmacological interventions) or if the measurement of MBF is to be combined with a metabolic or receptor study.

At present most $H_2{}^{15}O$ applications have utilised bolus injections (Bergmann *et al* 1984, 1989, Iida *et al* 1988), although the use of a slow infusion of $H_2{}^{15}O$ has been reported (Huang *et al* 1985). Recently, a new method was described where $H_2{}^{15}O$ was administered via continuous inhalation of $C^{15}O_2$ (Araujo *et al* 1991) which, under the influence of lung carbonic anhydrase, is essentially equivalent to a slow infusion of $H_2{}^{15}O$ (West and Dollery 1962). The slow administration reduces dead-time losses due to the high count rates encountered during the initial phase of bolus injections.

0143-0815/92/010001 + 20 $02.50

One difficulty associated with the quantitative measurement of MBF is the limited spatial resolution of PET scanners, resulting in the so called partial volume effect (Hoffman *et al* 1979). This is compromised even further by both cardiac and respiratory movements (Ter-Pogossian *et al* 1982). The high arterial concentration which occurs during $H_2{}^{15}O$ administration constitutes another problem. Due to the limited spatial resolution spill-over of activity from the heart chambers into the myocardial region of interest (ROI) may result.

In the present study eight different modifications of the same single-tissue compartment model (Kety 1951, 1960a, b) for kinetic analysis of $H_2{}^{15}O$ time-activity curves were applied to data obtained in both dogs and humans and then compared. The purpose of this analysis was to identify the model which would produce the most accurate and reproducible MBF results, accounting for potential underestimation of myocardial activity and possible cross contamination from the cardiac chambers.

2. Theory

As mentioned above, ^{15}O-labelled water is a metabolically inert tracer which, in the myocardium, is freely diffusible (Johnson *et al* 1952, Yipintsoi and Bassingthwaite 1970). Its behaviour in tissue can be described by the standard differential equation for a single tissue compartment model (Kety 1951, 1960a, b):

$$dC_t(t) / dt = F.C_a(t) - (F / V_d + \lambda).C_t(t) \tag{1}$$

where

$C_t(t)$ = regional tissue concentration of $H_2{}^{15}O$ (Bq per ml (tissue)) as function of time t,

$C_a(t)$ = arterial whole blood concentration of $H_2{}^{15}O$ (Bq per ml (blood)) as function of time t,

F = regional flow in ml (blood) per ml (tissue) min^{-1},

V_d = volume of distribution of water (ml (blood) per ml (tissue)),

λ = decay constant of ^{15}O (= 0.338 min^{-1}).

The solution to this differential equation is given by:

$$C_t(t) = F.C_a(t) \bullet \exp(-(F/V_d + \lambda).t) \tag{2}$$

where $\star$ indicates the convolution integral. $C_t(t)$ represents the tissue response to an arterial input function $C_a(t)$. Since radioactive decay has been incorporated in equations (1) and (2), both $C_a(t)$ and $C_t(t)$ should not be corrected for the decay of ^{15}O.

An alternative linearised (i.e. no convolution) solution to equation (1), as proposed by Blomqvist (1984), is

$$C_t(t) = F.\int_0^t C_a(\tau)d\tau - (F/V_d + \lambda).\int_0^t C_t(\tau)d\tau \tag{3}$$

In equations (1) to (3) the following assumptions are made:

(1) Both F and V_d are constant during the measurement period.

(2) Water is freely diffusible, i.e. the extraction fraction of water is unity and no binding of water in tissue occurs.

In practice it is not the actual tissue concentration which is measured, but rather the mean concentration within a (macroscopic) ROI. Such an ROI will contain not only tissue, but also blood. However, equations (1) to (3) would still provide a valid description for a macroscopic ROI if the following two additional assumptions are correct:

(3) Venous and tissue concentrations are the same, i.e. the effect of V_d not being equal to 1 is negligible.

(4) The contribution to the signal arising from arterial activity is negligible.

However, both myocardial blood volume (MBV) and its arterial fraction can not be neglected (Crystal *et al* 1981). In addition, due to the limited spatial resolution of PET scanners, the measured regional tissue concentration will be contaminated with a signal originating from the high level of activity present within the cardiac chambers (spill-over effect).

If the size of the ROI sampled is small and the thickness of the myocardium is large compared to the spatial resolution of the scanner, the contribution of arterial activity would best be described by:

$$C_{tot}(t) = (1 - V_a).C_t(t) + V_a.C_a(t) \tag{4}$$

where

$C_{tot}(t)$ = measured 'tissue' concentration in ROI (Bq per ml (ROI))

V_a = arterial blood volume (ml (arterial blood) per ml (ROI))

If, however, larger ROIs are employed, the spill-over signal will be higher than the signal from the local arterial vessels. In that case equation (4) should be replaced by

$$C_{tot}(t) = C_t(t) + V_{so}.C_a(t) \tag{5}$$

where V_{so} now represents the arterial spill-over fraction.

The limited resolution of PET scanners might not only result in the inclusion of spill-over activity, but also in an underestimation of the regional tissue concentration $C_t(t)$ (partial volume effect (Hoffman *et al* 1979)). This effect is further enhanced by the presence of both cardiac and respiratory movements (Ter-Pogossian *et al* 1982). The resulting underestimation in F and V_d will be identical. One method to deal with this partial volume effect and losses due to cardiac wall motion is to include a component for the fraction of water exchanging tissue, originally suggested by Iida *et al* (1988), as follows:

$$F = \alpha.F' \tag{6}$$

$$V_d = \alpha.p \tag{7}$$

where

α = fraction of water exchanging tissue (ml (water exchanging tissue) per ml (ROI))

p = partition coefficient of water (ml (blood) per ml (water exchanging tissue))

F' = flow for the water exchanging tissue (ml (blood) per ml (water exchanging tissue) min^{-1}).

It should be noted, that α represents the fraction of tissue within the ROI which is capable of exchanging water within the time course of the measurement. Consequently, F' represents blood flow for this fraction of water exchanging tissue within the ROI rather than for the entire ROI. In equation (7) it has been assumed that the volume of distribution of water for the water exchanging tissue is the same as the partition coefficient of water for (normal) myocardial tissue. Substituting equations (6) and (7) in equations (2) and (3) respectively results in:

$$C_t(t) = \alpha.F'.C_a(t) * \exp[-(F'/p + \lambda).t] \tag{8}$$

$$C_t(t) = \alpha.F'.\int_0^t C_a(\tau)d\tau - (F'/p + \lambda).\int_0^t C_t(\tau)d\tau \tag{9}$$

Based on the theory given above, eight different operational equations can be defined, by utilising four different descriptions of C_t with two different methods to incorporate

arterial blood volume. An overview of the different operational equations is given in table 1. The difference between V_a and V_{so} models is schematically illustrated in figure 1, that between V_d and α models in figure 2.

Table 1. Overview of tested models.

Model	Operational equation
1	$C_{tot}(t) = (1 - V_a).\{F.C_a(t) \star \exp[-(F/V_d + \lambda).t]\} + V_a.C_a(t)$
2	$C_{tot}(t) = F.C_a(t) \star \exp[-(F/V_d + \lambda).t]\} + V_{so}.C_a(t)$
3	$C_{tot}(t) = (1 - V_a).\{\alpha.F'.C_a(t) \star \exp[-(F'/p + \lambda).t]\} + V_a.C_a(t)$
4	$C_{tot}(t) = \alpha.F'.C_a(t) \star \exp[-(F'/p + \lambda).t]\} + V_{so}.C_a(t)$
5	$C_{tot}(t) = [(1 - V_a).F + V_a.(F/V_d + \lambda)] \int_0^t C_a(\tau)d\tau - (F/V_d + \lambda) \int_0^t C_{tot}(\tau)d\tau + V_a.C_a(t)$
6	$C_{tot}(t) = [F + V_{so}.(F/V_d + \lambda)] \int_0^t C_a(\tau)d\tau - (F/V_d + \lambda) \int_0^t C_{tot}(\tau)d\tau + V_{so}.C_a(t)$
7	$C_{tot}(t) = [\alpha.(1 - V_a).F' + V_a.(F'/p + \lambda)] \int_0^t C_a(\tau)d\tau - (F'/p + \lambda) \int_0^t C_{tot}(\tau)d\tau + V_a.C_a(t)$
8	$C_{tot}(t) = [\alpha.F' + V_{so}.(F'/p + \lambda)] \int_0^t C_a(\tau) - (F'/p + \lambda) \int_0^t C_{tot}(\tau)d\tau + V_{so}.C_a(t)$

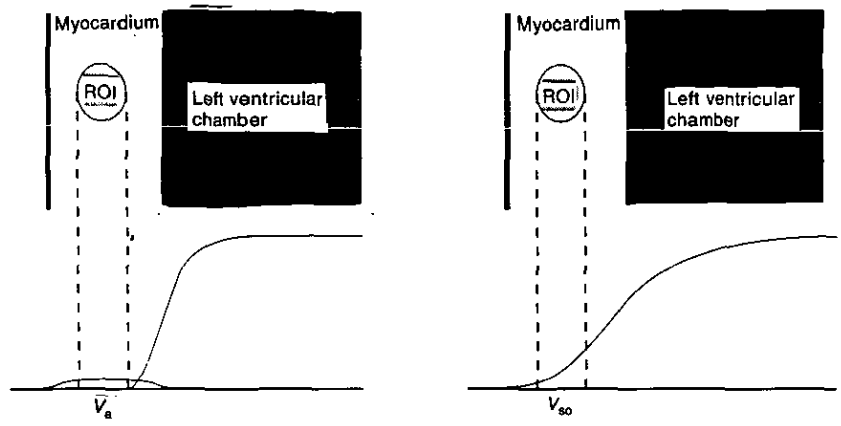

Figure 1. Schematic illustration of the difference between V_a (left) and V_{so} (right) models. In the V_a models the arterial signal component within the ROI is assumed to be entirely due to the regional arterial blood volume V_a with the spill-over signal from the left ventricle being negligible. The volume V_a should, therefore, be taken into account in attributing the tissue signal to a certain volume, resulting in equation (4) in the text. In contrast, in the V_{so} models, the arterial signal is assumed to originate entirely from spill-over activity, i.e. the regional arterial signal is negligible compared to the spill-over component, resulting in equation (5) in the text. It should be noted that, in practice, a combination of both blood signals will be present. However, since the time course of both signals is the same, it is not possible to discriminate between them and consequently, in fitting, one of the models has to be selected.

$C_a(t)$ (left atrium and/or ventricle) and $C_{tot}(t)$ (myocardium) can be measured non-invasively as a function of time with dynamic PET scanning (Weinberg *et al* 1988, Araujo *et al* 1991). Using standard non-linear regression analysis the operational equation can then be fitted for F, V_d or α, F' and V_a or V_{so} depending on the actual model used. In the models containing α, a value for p has to be assumed. From *in vitro* water content data for blood and myocardial tissue (Altman and Dittmer 1971, ICRP 1974) a partition coefficient of water of 0.96 ml ml^{-1} can be calculated for the myocardium which was the value used in the present study. This value is in agreement with the values of 0.91 g ml^{-1} and 0.92 g ml^{-1} used by Iida *et al* (1988) and Bergmann *et al* (1989), respectively, taking into account the density of myocardial tissue (1.04 g ml^{-1}).

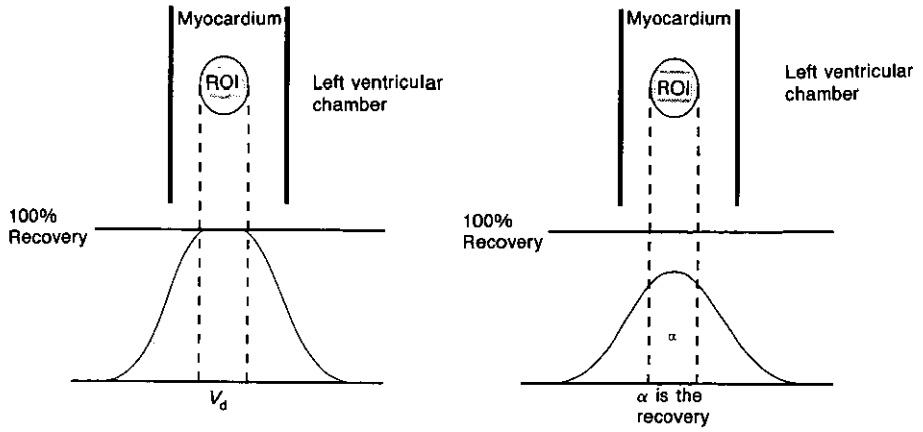

Figure 2. Schematic illustration of the difference between V_d (left) and α (right) models. If there is full count recovery within an ROI, a V_d model would be more appropriate, since it avoids any assumptions regarding the volume of distribution of water. However, if the recovery is less than 100% an α model would be a better choice, since, by definition, it incorporates a component to account for this loss of recovery. Such a model does, however, require an assumed value for the volume of distribution of water.

As an alternative to fitting for three parameters, MBV can be measured separately and subtracted from the tissue data before fitting or it can be fixed to the measured value in the fitting process. This would reduce the number of parameters to be estimated in the regression analysis to two, but would introduce an inaccuracy by treating the venous blood volume as being at arterial concentration, due to equilibration of $C^{15}O$ in the blood pool.

3. Methods

Data were obtained in 8 dogs and 11 normal subjects during resting conditions and following pharmacological interventions. The purpose of these pharmacological interventions was to alter MBF and hence provide a means of testing the various models over a wider flow range.

3.1. Scanning protocol

For both animal and human studies use was made of an ECAT 931-08/12 (CTI Inc., Knoxville, TN, USA) positron emission tomograph (Spinks *et al* 1988). First, a short rectilinear transmission scan was performed in order to optimise positioning of the heart in the centre of the field of view. This was followed by acquisition of a transmission scan for the purpose of attenuation correction of all subsequent emission scans.

Following the transmission scan a blood pool scan was performed using $C^{15}O$. The $C^{15}O$ gas was inhaled for 4 min at a concentration of 3 MBq ml^{-1} and a flow rate of 500 ml min^{-1}. One minute after the end of inhalation, to allow for equilibration (Martin *et al* 1987), a single scan with a duration of 6 min was acquired. Arterial (dogs) or venous (humans) blood samples were collected 0, 2, 4 and 6 min after the start of scanning. After ^{15}O levels had fallen to background levels, in humans, a base-line MBF study was performed. Sequential dynamic scans (frames) were collected over a period of 7 min according to the following protocol: 1 (background) frame of 30 s, 6 of 5 s, 6 of 10 s, 6 of 20 s and 6 of 30 s. Subjects inhaled a constant supply of $C^{15}O_2$ for a period of 3.5 min beginning at the start of the second frame. $C^{15}O_2$ gas was delivered at a concentration of 3 to 5 MBq ml^{-1} and a flow rate of 500 ml min^{-1}. The first frame of 30 s was introduced as a means of monitoring and correcting for residual tissue activity.

When residual ^{15}O activity had fallen to background levels, in humans, a repeat MBF study was performed following administration of dipyridamole. The scanning and gas administration protocol were identical to those used for the base-line studies.

Although identical scanning and gas administration p `ocols were used in dogs, the order of MBF studies was variable. A variable amount of dipyridamole was utilised and in one dog morphine was given in an attempt to cover also intermediate and reduced flow rates.

All emission scans were reconstructed using a Hanning filter with a cut-off frequency 0.5 of maximum. This resulted in a spatial resolution of 8.4 × 8.3 × 6.6 mm^3 FWHM (full width at half maximum) at the centre of the field of view (Spinks *et al* 1988).

3.2. Animal studies

The method was validated in eight fasting greyhound dogs with weights ranging from 28 to 35 kg. Anaesthesia was induced with intravenous sodium pentobarbital (25 mg kg^{-1}). The dogs were then intubated and mechanically ventilated with an N_2O/O_2/air mixture. Anaesthesia was maintained using halothane (0.5 - 1%). Catheters were advanced via the femoral artery into the descending aorta for withdrawal of arterial blood samples and into the left ventricle for the measurement of left ventricular pressure and injection of radiolabelled microspheres. A catheter was inserted into the femoral vein for continuous infusion of an isotonic dextrose/saline solution and for the administration of drugs. An electrocardiogram was continuously recorded for the duration of the study.

Regional MBF measurements were made at rest (n = 5) and following a 4 min intravenous infusion of 0.30 to 0.56 mg kg^{-1} dipyridamole (n = 7) or a 3 min intravenous infusion of 3 mg morphine (n = 1). These drugs were used in order to raise or lower MBF respectively. In all cases PET scanning started 2 min after the end of drug infusion.

Two minutes after the start of each $C^{15}O_2$ run, 15 μm diameter microspheres were infused into the left ventricle over a period of 30 s. Microspheres were labelled with ^{113}Sn, ^{95}Nb, ^{46}Sc or ^{57}Co. Continuous withdrawal of femoral arterial blood at a flow rate of 5.12 ml min^{-1} using a Harvard pump was started at the beginning of microsphere infusion and continued for 2 min after the end of infusion. At the end of the experiments, the dogs were sacrificed by intravenous injection of an overdose of sodium pentobarbital and the hearts extracted and dissected regionally. These tissue samples were weighed and together with the corresponding arterial blood samples counted in a gamma counter (Wallak Ultragamma 2).

3.3. Human studies

Human studies were performed in 11 healthy normal male subjects with an age ranging from 26 to 42 years. No subject had signs or symptoms of cardiac disease. A Venflon cannula was advanced into an antecubital vein for the withdrawal of venous blood samples and for the infusion of coronary vasodilators.

MBF measurements were performed at base-line and following infusion of dipyridamole (0.56 mg kg^{-1}) over a period of 4 min. $C^{15}O_2$ scans were initiated 2 min after the end of infusion. As a precaution, aminophylline was readily available to reverse the effects of dipyridamole.

All normal subjects gave written informed consent prior to scanning. The studies were approved by the Research Ethics Committee of Hammersmith Hospital. Permission to administer the radioactive tracers was obtained from the United Kingdom Administration of Radioactive Substances Advisory Committee.

3.4. Data analysis

After reconstruction, all images were transferred to a workstation (Sun 3/60, Sun Microsystems, Mountain View, USA).

A functional image of myocardial blood volume (MBV) was generated by dividing the $C^{15}O$ image by the average concentration of the blood samples (both image and samples corrected for decay) on a pixel by pixel basis. The MBV image was used to define a number of ROIs, positioned over the left atrium, with a mean (±SD) size of 2.2 ± 0.6 cm^3 for dog and 2.1 ± 0.7 cm^3 for human studies. Of these ROIs only those (3 to 5) with an MBV value greater than 0.9 ml (blood) per ml (ROI) (i.e. a recovery coefficient $> 90\%$) were projected onto the dynamic $C^{15}O_2$ images in order to generate left atrial time-activity curves. The average of these atrial curves was in turn used as the arterial input function for the subsequent kinetic MBF analysis. A similar procedure was followed to produce a second arterial input function based on ROIs positioned over the left ventricle. In this case the mean size was 3.3 ± 0.9 cm^3 for dog and 2.8 ± 1.0 cm^3 for human studies. As for the atrium, only those ROIs with a recovery coefficient $> 90\%$ were accepted for further analysis, thereby reducing spill-over contamination from the myocardium into the blood curve.

A second functional image was generated for the definition of tissue ROIs. This (washout) image was produced by adding the last three frames of the dynamic $C^{15}O_2$ scanning sequence and subtracting the MBV image described above (Araujo *et al* 1991). Although a flow component will be present, the washout image will primarily be determined by the tissue volume of distribution of water. Routinely, a number of circular (10 mm radius) ROIs were defined for the myocardium, taking care that the position of each ROI was centred within the myocardial wall as assessed from the washout image. These ROIs were projected on to the dynamic $C^{15}O_2$ images to produce tissue time-activity curves. For the subsequent kinetic analysis average tissue response curves were generated for the anterior, lateral and inferior segments of the left ventricle and for the septum based on the position of the original ROIs.

In two studies (one dog, one human) additional tissue time activity curves were generated in a similar fashion, but with varying size and positioning of the original ROIs. The purpose of this analysis was to test the stability of the various models with respect to size and positioning of the ROIs, thereby providing an indirect assessment of reproducibility. The radius of centred circular ROIs was varied from 4 to 20 mm. In addition, a number of circular (4 to 10 mm radius) ROIs were defined such that their centres were located either on the inner or the outer edge of the myocardium. Finally, parallel elliptical ROIs (short axis = 4 mm perpendicular to the myocardium; long axis = 20 mm) were defined on one dog study, with the innermost ROI positioned entirely within the left ventricular chamber and the outermost ROI in the lung.

Selected studies were refitted with V_a fixed to the MBV value obtained from the $C^{15}O$ analysis.

In the dog studies MBF was also calculated from the microsphere data using the standard reference technique (Heymann *et al* 1977). In the comparison of MBF obtained from PET and microsphere data a correction was made for the density of myocardial tissue (1.04 g ml^{-1}) since they are expressed per ml and per g of tissue respectively.

In the regression analysis no weighting was applied to account for possible uneven noise levels of different frames. It should be noted, however, that proper weighting factors are not simply related to the recorded counts within an ROI, but primarily to the activity within the total field of view of the scanner. Selected studies were therefore also fitted using weighting factors which were based on the total count rate of the scanner. These fits

provided MBF results which were not significantly different from those of the unweighted fits. Although this finding indicates that the results are not very sensitive to changes in weighting, further studies will be required to determine the optimal weighting factors.

4. Results

4.1. Animal studies

In figures 3 and 4 MBF data are related to microsphere flow for all eight models, respectively using the left atrium and the left ventricle as an input function. Results of the linear regression analyses are given in table 2. For both input functions a good correlation can be observed for all convolution models (1 to 4), with a poorer correlation for the linearised models (5 to 8). Average values for V_d, α, V_a and V_{so} are shown in table 3.

The effects of size and position of the original ROIs (schematically illustrated in figure 5) on the fitted parameters are shown in figure 6 (only data for models 1 to 4 illustrated) for the anterior wall. Similar results were obtained for the lateral and the postero-inferior walls. In terms of stability of MBF, of all eight models, best results were obtained for models 3 and 4 (i.e. the convolution models which include a component for the fraction of water exchanging tissue), the main effects of increasing ROI size being a decrease in α and an increase in V_a or V_{so}.

In figure 7 (data for models 1 to 4 only illustrated) the effect of ROI position using large elliptical ROIs, as schematically illustrated in figure 8, is demonstrated, with models 1, 3 and 4 giving the most stable results. It is clear, however, that a shift towards the ventricle is associated with less change in MBF than a shift towards the lung.

Table 2. Linear regression of MBF with microsphere flow.

Model*	Slope**	Intercept** (ml ml^{-1} min^{-1})	Correlation coefficient
1a	0.95±0.06	0.28±0.20	0.91
2a	1.00±0.06	0.02±0.21	0.91
3a	0.96±0.06	0.36±0.20	0.91
4a	0.96±0.06	0.36±0.20	0.91
5a	0.49±0.08	0.72±0.25	0.68
6a	0.36±0.07	0.65±0.23	0.56
7a	0.50±0.07	0.80±0.23	0.71
8a	0.50±0.07	0.80±0.22	0.71
1v	1.04±0.07	−0.08±0.23	0.92
2v	1.06±0.07	−0.31±0.22	0.93
3v	1.04±0.06	−0.03±0.22	0.93
4v	1.04±0.06	−0.03±0.22	0.93
5v	0.68±0.09	0.35±0.30	0.76
6v	0.57±0.09	0.30±0.30	0.69
7v	0.68±0.08	0.41±0.28	0.78
8v	0.68±0.08	0.41±0.29	0.78

* a indicates left atrial (N = 52), v left ventricular (N = 44) input.

** Values ± standard errors are given.

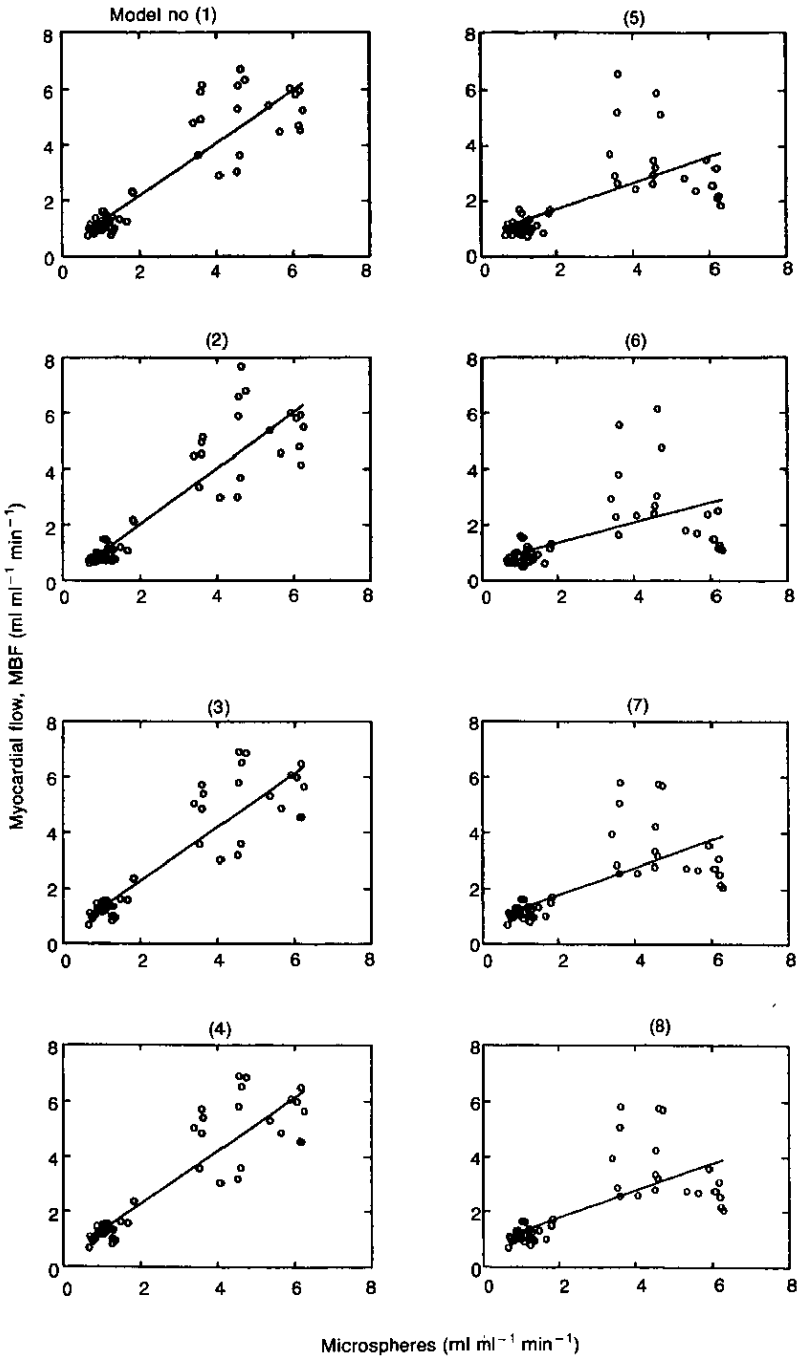

Figure 3. Comparison of MBF obtained from the eight different models listed in table 1, using the left atrium for the definition of the input function, with microsphere flow. The lines correspond to the best fits of the linear regression analyses.

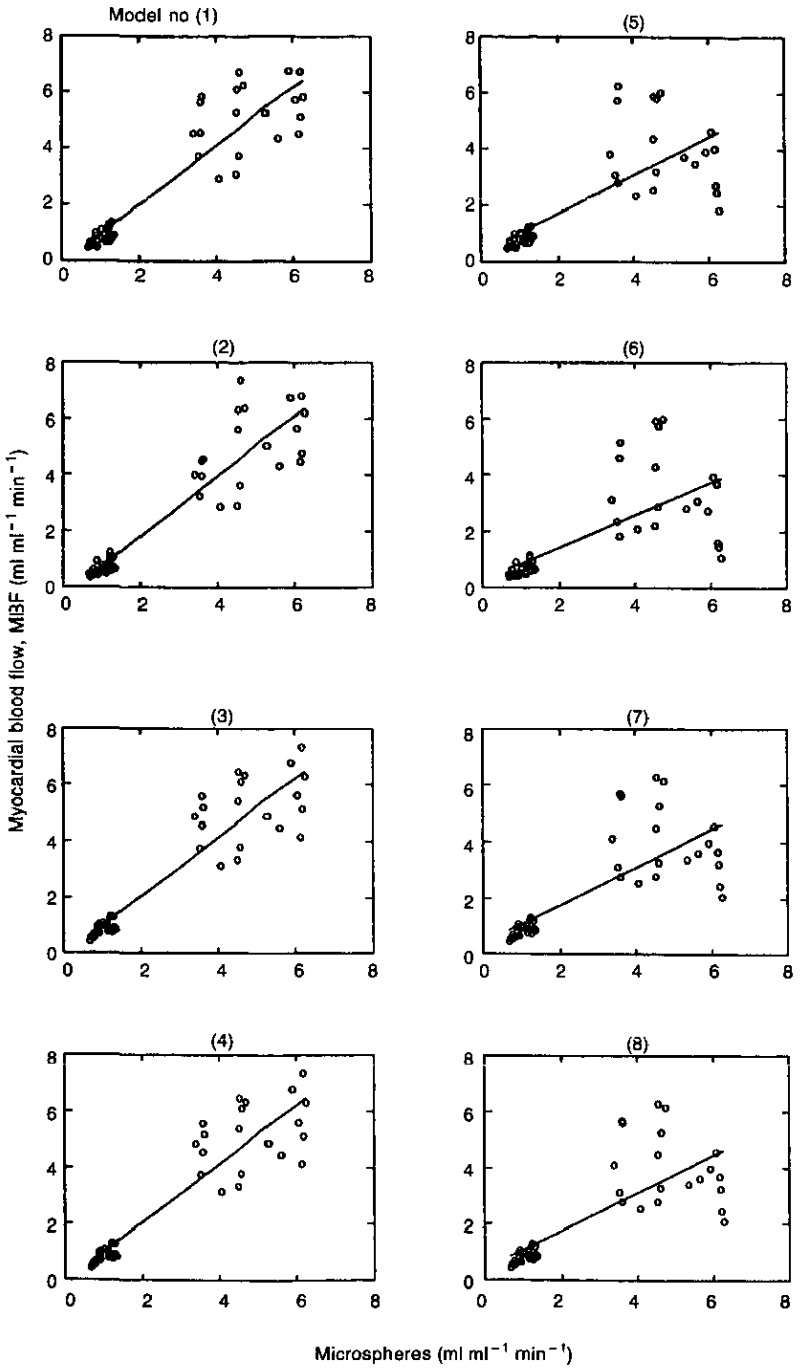

Figure 4. Comparison of MBF obtained from the eight different models listed in table 1, using the left ventricle for the definition of the input function, with microsphere flow. The lines correspond to the best fits of the linear regression analyses.

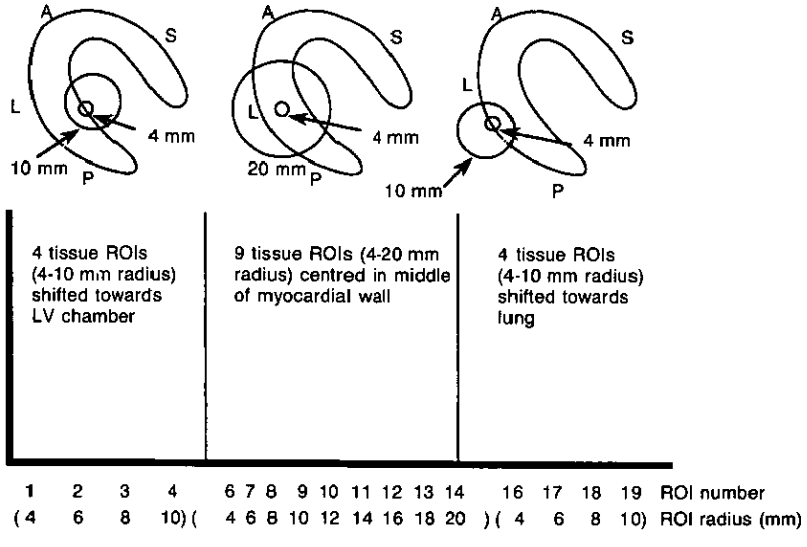

Figure 5. Schematic illustration of the numbering of the ROIs used in the analyses of the effects of size and position shown in figures 6, 8 and 9.

4.2. Human studies

A similar analysis to that shown in figure 6 for dogs is given in figures 9 and 10, for base-line and dipyridamole lateral wall data respectively. Again, from the eight models tested, convolution models 3 and 4, which include a parameter for the fraction of water exchanging tissue, provide the most stable results. The main difference between these two models are

Table 3. Mean values (±SD) of V_d, α, V_a and V_{so} in dog studies.

Model*	V_d (ml ml^{-1})	α (ml ml^{-1})	V_a (ml ml^{-1})	V_{so} (ml ml^{-1})
1a	0.90±0.08		0.10±0.12	
2a	0.81±0.14			0.10±0.12
3a		0.94±0.09	0.10±0.12	
4a		0.85±0.15		0.10±0.12
5a	0.90±0.09		0.21±0.13	
6a	0.71±0.14			0.21±0.13
7a		0.94±0.09	0.21±0.13	
8a		0.74±0.15		0.21±0.13
1v	0.92±0.11		0.12±0.12	
2v	0.82±0.15			0.12±0.12
3v		0.96±0.11	0.12±0.12	
4v		0.85±0.16		0.12±0.12
5v	0.92±0.11		0.19±0.12	
6v	0.75±0.15			0.19±0.12
7v		0.96±0.11	0.19±0.12	
8v		0.78±0.15		0.19±0.12

* a indicates left atrial (N = 52), v left ventricular (N = 44) input.

the more realistic values for the fraction of water exchanging tissue obtained with model 4 (i.e. the model which treats the blood contribution as being due to spill-over from the cardiac chambers), especially for ROIs which are centred on the inner edge of the myocardium.

Mean values of MBF, α and V_{so}, as obtained with model 4, for six normal subjects are given in table 4 for both left atrial and left ventricular input functions. As for dogs (table 3) there was no significant difference in α and V_{so} estimates obtained from atrial and ventricular input functions. Left atrial input functions provide a somewhat lower intersubject variability than left ventricular input functions. As an index of regional variability for each of the six subjects the coefficient of variation (COV) of MBF over the four regions was calculated. Mean values of this analysis are given in table 5. It can be seen that the variability is less for atrial than for ventricular input functions, especially in the dipyridamole studies. A paired t-test applied to the base-line data showed not a significant difference ($P = 0.267$). For the dipyridamole studies, however, the significance level was $P = 0.037$.

In figure 11 a fit, according to model 4, for MBF, α and V_{so} is compared to a similar fit for MBF and α, but with V_{so} fixed to the MBV value obtained from the $C^{15}O$ scan. The quality of the latter fit is clearly inferior. This was also reflected in the MBF values with the three parameter fit resulting in an MBF value similar to microsphere flow, but with the two parameter fit producing an MBF value which was a factor of two lower. In addition, standard errors of MBF and α were higher if MBV was subtracted prior to fitting.

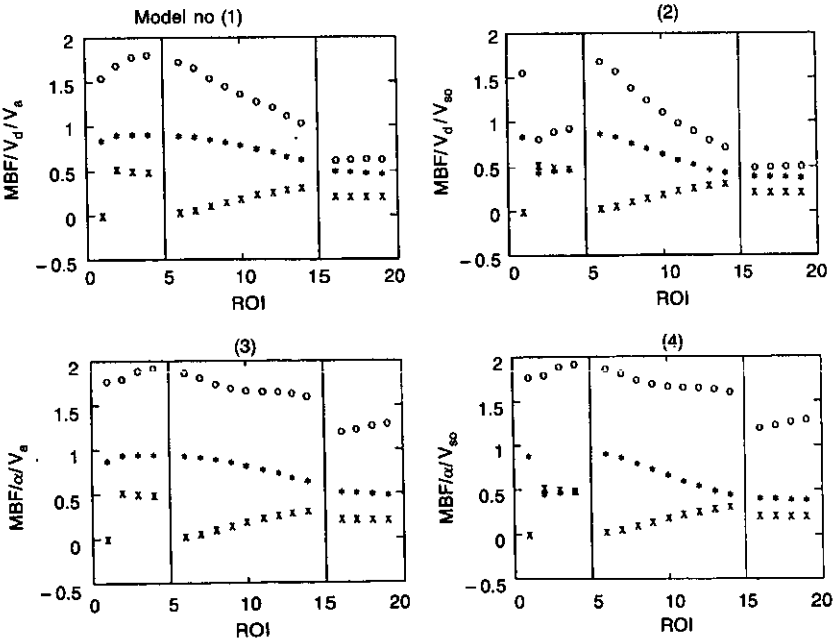

Figure 6. Effects of size and position of the original ROIs on the fitted parameters of models 1 to 4 in one of the dog studies. The numbering of the ROIs is as shown in figure 5. (o) represents MBF, (*) represents V_d or α and (x) represents V_a or V_{so}.

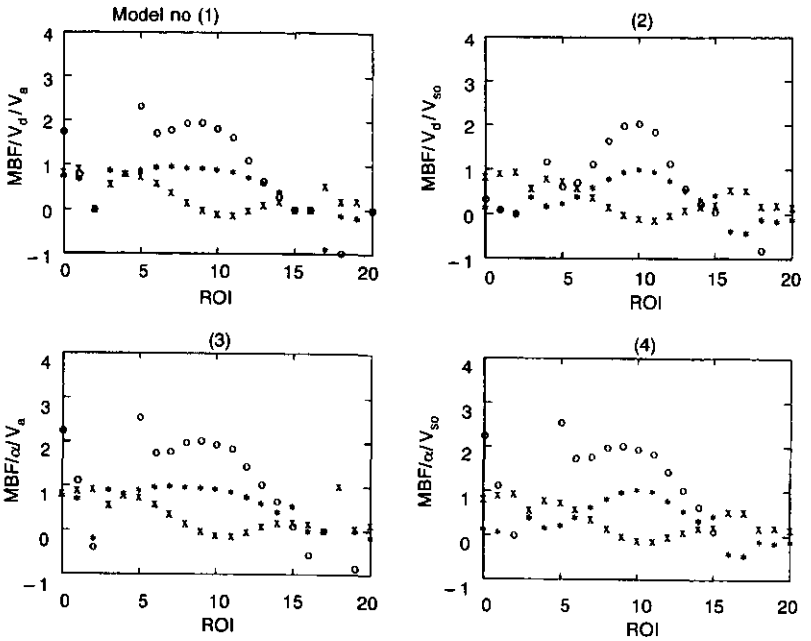

Figure 7. Effect of the position of large elliptical ROIs on the fitted parameters of models 1 to 4. ROIs are shifted from being located entirely within the left ventricle (ROI 0) to being located entirely within the lung (ROI 20), with the most centred position for ROI 10, as schematically illustrated in figure 8. The symbols are identical to those used in figure 6.

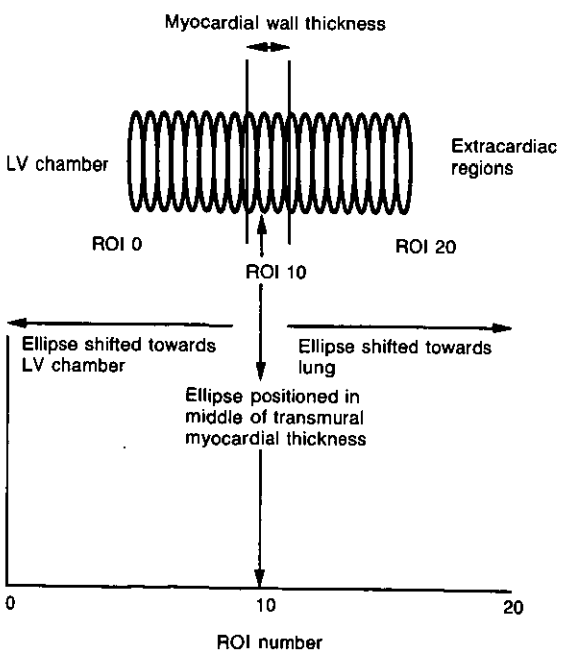

Figure 8. Schematic illustration of the numbering of the large elliptical ROIs used in the analyses of the effects of position shown in figure 7.

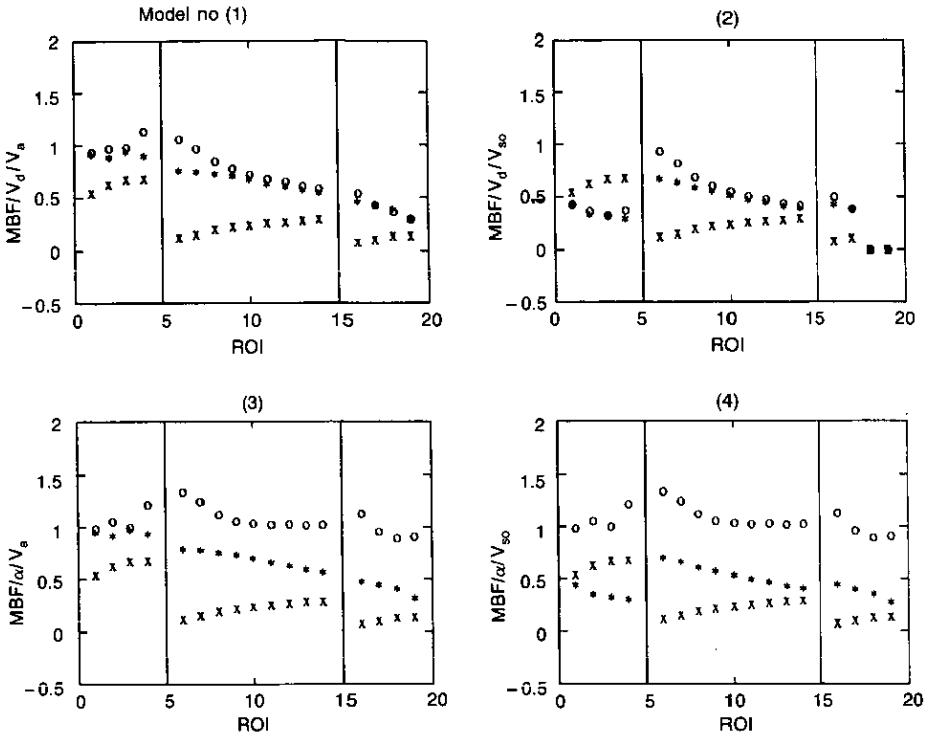

Figure 9. Effects of size and position of the original ROIs on the fitted parameters of models 1 to 4 in a baseline human study. The numbering of the ROIs is as shown in figure 5. The symbols are identical to those used in figure 6.

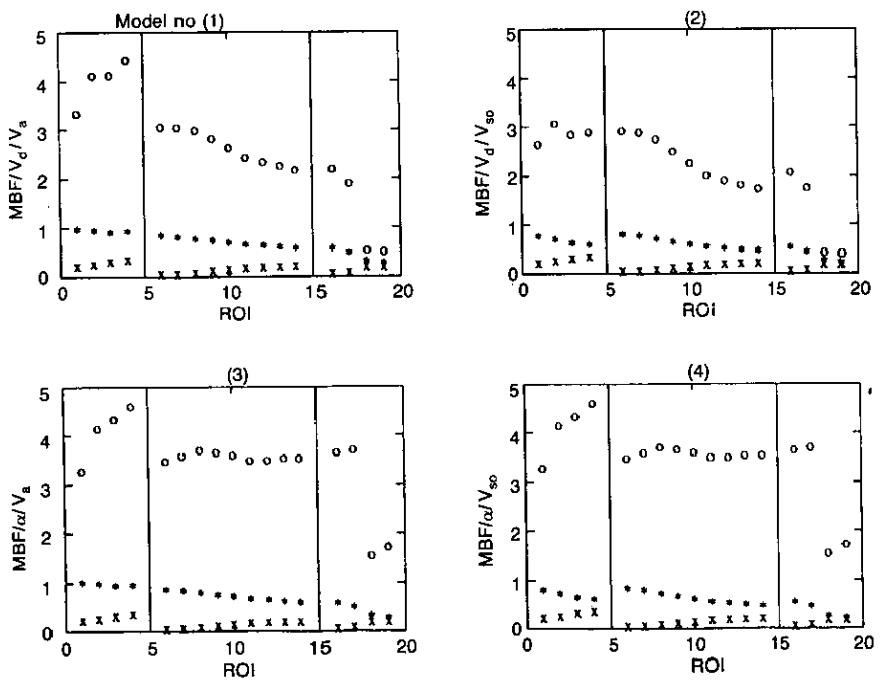

Figure 10. Effects of size and position of the original ROIs on the fitted parameters of models 1 to 4 in a dipyridamole human study. The numbering of the ROIs is as shown in figure 5. The symbols are identical to those used in figure 6.

Table 4. Mean values (±SD) for model 4 in six normal subjects.

ROI	MBF (ml ml^{-1})	α (ml ml^{-1})	V_{so} (ml ml^{-1})
Left atrium, base-line			
Anterior	0.92±0.13	0.58±0.06	0.20±0.03
Inferior	0.94±0.11	0.55±0.05	0.25±0.03
Lateral	1.00±0.17	0.58±0.08	0.22±0.03
Septum	0.83±0.16	0.74±0.11	0.25±0.06
Left ventricle, base-line			
Anterior	0.96±0.14	0.56±0.05	0.22±0.03
Inferior	1.00±0.19	0.53±0.06	0.28±0.04
Lateral	1.04±0.23	0.56±0.06	0.25±0.03
Septum	0.86±0.18	0.72±0.10	0.28±0.07
Left atrium, dipyridamole			
Anterior	4.23±0.60	0.69±0.15	0.13±0.10
Inferior	4.24±0.79	0.67±0.08	0.14±0.04
Lateral	4.60±1.20	0.66±0.12	0.14±0.05
Septum	4.22±0.92	0.85±0.17	0.16±0.12
Left ventricle, dipyridamole			
Anterior	4.73±0.98	0.63±0.10	0.18±0.05
Inferior	4.58±1.51	0.58±0.10	0.24±0.13
Lateral	5.16±1.89	0.59±0.10	0.21±0.09
Septum	4.51±1.50	0.75±0.03	0.26±0.04

Table 5. Mean intrasubject regional COV for model 4.

Left atrium, base-line	15.2%
Left ventricle, base-line	16.2%
Left atrium, dipyridamole	10.1%
Left ventricle, dipyridamole	16.4%

5. Discussion

^{15}O labelled H_2O has the advantage over other currently available tracers of regional MBF (e.g. $^{13}NH_3$ and ^{82}Rb) in that its uptake in myocardial tissue is independent of metabolism. Therefore, in theory, it is the most reliable tracer in metabolically impaired myocardium. In addition, the short half-life of ^{15}O makes it an attractive tracer if more than one study within a single scanning session are required such as measurements of MBF before and after administration of dipyridamole.

An important disadvantage of $H_2{}^{15}O$ is its high arterial concentration. In the present study eight different tracer models were compared, with each model incorporating an intrinsic correction for the contribution of arterial activity to the 'measured' myocardial concentration. It should be realised, however, that there are some implicit assumptions common to all models.

Firstly, it is assumed that both MBF and the volume of distribution of ^{15}O-labelled water are constant during the study period. This is a standard requirement for all practical PET techniques. It is a reasonable assumption for base-line studies, but some inaccuracies might occur in challenge studies such as following dipyridamole injection. This illustrates the

advantage of minimising the scanning period as much as possible. It should be noted that in the present study only one scanning protocol was assessed. Although it is likely that the comparative results also hold for other protocols, further studies will be required to optimise the scanning protocol.

A second assumption common to all models is that the extraction fraction of water is unity. Although it has been shown that there are some diffusion limitations for water in the brain (Eichling *et al* 1974, Paulson *et al* 1977, Go *et al* 1981, Lammertsma *et al* 1981, Herscovitch *et al* 1987), this effect should be negligible in the myocardium due to the much larger permeability surface area product of myocardial tissue. For the myocardium the permeability P has been estimated to be 6×10^{-4} cm s^{-1} (Rose *et al* 1977), whilst the estimated values of the surface area S for the myocardium range from 730 to 1260 cm^2 ml^{-1} (Altman and Dittmer 1971). Therefore the PS product will range from 3091 to 5336 ml dl^{-1} min^{-1}. Using these products, it can be calculated that even for a flow as high as 8 ml ml^{-1} min^{-1}, the extraction fraction for water will be at least 98%.

In compartmental analysis of ROI data it is usually assumed that for freely diffusible tracers such as water, venous and tissue activity can be treated as a single compartment. This is a valid assumption if the volume of distribution of the tracer in tissue is unity. From *in vitro* water content data for blood and myocardial tissue (Altman and Dittmer 1971, ICRP 1974) a partition coefficient of water of 0.96 ml ml^{-1} can be calculated for the myocardium. The resulting error in flow for such a value is negligible (Koeppe *et al* 1987). However, this assumption could potentially be compromised in the V_d models (models 1, 2, 5 and 6).

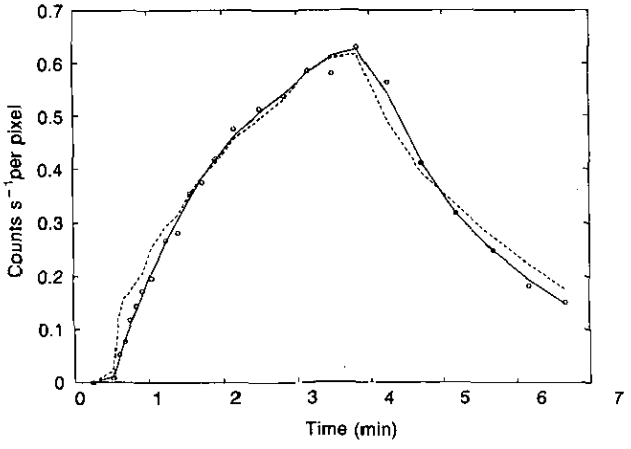

Figure 11. Measured time activity curve (o) for an ROI positioned over the septum of a normal subject. The solid line represents the best fit for MBF, α and V_{so} according to model 4. The dashed line represents a similar fit with V_{so} fixed to the value obtained from the measurement of MBV.

5.1. Comparison of models

In dogs, good correlation between MBF and microsphere flow was obtained for all convolution models (models 1 to 4; figures 3 and 4, table 2). The performance of the linearised models (models 5 to 8) was significantly worse (see, for example, slope and correlation coefficient in table 2), especially for increased flow rates. Although the latter models are approximations (Blomqvist 1984), they would have been interesting from a computational point of view. In addition, they would have allowed direct fitting of sinograms. However, it is clear that the results obtained with these linearised models in the

present study are not satisfactory. The poorer performance of these linearised models is mainly due to a higher degree of scatter at high flow rates, where arterial and tissue curves become more similar and the regression analysis becomes more sensitive to small errors. For the linearised models, at any time point, both arterial and tissue concentrations and their integrals are required. The limited time resolution of practical PET scans requires that values for either the instantaneous or the integral concentrations need to be interpolated. Apparently, in the present study, this interpolation resulted in errors which were amplified at high flow rates. For successful application of the linearised models, further studies will be required to optimise the interpolation procedure.

In order to avoid interobserver variability, for clinical applications MBF results should not be too sensitive to the actual positioning of the ROIs. From the analysis illustrated in figures 6, 7, 8 and 10 it followed that best stability was obtained for models 3 and 4, incorporating the fraction of water exchanging tissue. It is of interest to note that a shift towards the chamber had less severe implications than a shift towards the lung. This is probably due to the fact that none of the models incorporated a contribution from lung radioactivity which is at a different concentration.

Although models 3 and 4 provided similar MBF results, in human studies model 4 seemed to be more realistic. The low fractions of water exchanging tissue, in agreement with previously published data (Iida *et al* 1988), implied that a major part of the blood contribution should be due to spill-over activity. This is especially the case for ROIs shifted towards the left ventricle (ROIs 1 to 4 in figures 6, 8 and 10).

It is of interest to note that for human studies α is lower and V_{so} is higher than for the dog studies. This is consistent with the fact that the myocardial wall in greyhounds is substantially thicker than that in man (Araujo *et al* 1991).

It should be realised that the fraction of water exchanging tissue obtained with model 4 not only serves as a correction factor, but also has potential as a physiological parameter of interest in its own right. For example, in infarction, a reduction in α might be expected. However, the remaining (water exchanging) tissue could have normal MBF. In contrast, in pure ischaemia, a reduced MBF with normal α would be expected. However, further studies will be required to assess theses hypotheses. It should be noted that the values of α in the septum tend to be higher than those for the other myocardial regions. This is most likely due to spill-over activity from the right ventricle, which is at venous concentration. This spill-over signal will, therefore, be more similar to the tissue than to the arterial signal, resulting in an apparent increase in the fraction of water exchanging tissue.

Left atrial and left ventricular input functions provided similar MBF values in both dog and human studies. However, due to the lower intrasubject variation in human studies, at present preference should be given to the left atrium as a site for defining the arterial input function. The left ventricle is probably more affected by spill-over of myocardial activity, especially in dipyridamole studies. Although, in theory, a correction can be made for the latter spill-over effect (Iida *et al* 1990), preliminary studies (data not shown) have not shown a significant improvement. A potentially more accurate technique would be external detection of continuously withdrawn arterial blood (Iida *et al* 1988), as routinely employed in cerebral blood flow studies (Lammertsma *et al* 1990). However, definition of the arterial input function from the left atrium (or ventricle) has the important advantage that cannulation of the radial artery can be avoided. In addition, external detection would require corrections to be made for delay and dispersion of the measured input function (Lammertsma *et al* 1990). The present study provides further evidence that the input function can be defined from the scans themselves, as previously demonstrated by Weinberg *et al* (1988). In this respect an independent $C^{15}O$ scan is useful in ensuring sufficient recovery of arterial ROIs.

The main disadvantage of model 4 is that it has to be assumed that p (i.e. the water content ratio) of myocardial tissue is constant. Further studies will be required to assess if this assumption holds in various pathological conditions, especially where this would result in heterogeneous tissue composition within ROIs. In this respect it should be noted that in brain studies it has been demonstrated that flow and distribution volume of water have different sensitivities to tissue heterogeneity (Lammertsma *et al* 1990). However, at least in predominantly normal tissue, this potential drawback is compensated by the major advantage that the obtained MBF value is independent of limitations of spatial resolution.

Theoretically, the statistical precision of MBF could be improved by limiting the number of parameters to be fitted. One option is subtracting blood volume (using the $C^{15}O$ scan) prior to fitting or alternatively to fix the blood volume component to this measured value. However, this would treat the venous blood volume as being at arterial concentration. Comparison of three and two parameter fits in selected cases demonstrated poorer fits for the two parameter approach as shown in figure 11. In addition, especially in the septum, MBF was grossly underestimated with the two parameter fit. It is of interest to note that in the latter case even the standard error of MBF deteriorates due to the poorer fit.

6. Conclusions

The present study has demonstrated the accuracy of myocardial blood flow measurements using inhalation of $C^{15}O_2$ and positron emission tomography.

Several variations of the same tracer kinetic model provide similar results in animal studies. However, in humans, preference should be given to a model incorporating MBF, a fraction of water exchanging tissue and a spill-over blood volume component. This model assumes that the water content of myocardial tissue is constant. Further studies are required to validate this assumption. Linearisation of the operational equation of this model does not provide satisfactory results.

Use of an arterial input function obtained from ROI analysis of the left atrium provides slightly better inter- and intrasubject regional variation than that obtained from the left ventricle. However, care should be taken in ensuring sufficient count recovery within the ROIs used.

Fitting of an arterial blood volume component from the data is superior over an independent measurement of (total) blood volume.

Further studies will be required to determine the best route of administration of the tracer, i.e. infusion of $C^{15}O_2$ as against infusion of $H_2{}^{15}O$, and to establish the optimal input function (e.g. infusion versus bolus).

Acknowledgements

We would like to thank the staff of the MRC Cyclotron Unit for their invaluable support, in particular the cyclotron and radiochemistry staff for the production of $C^{15}O_2$, Claire Taylor and Graham Lewington for technical assistance during scanning and members of the Clinical Section for providing data from normal subjects, who were scanned as part of an ongoing clinical programme. Ranil de Silva is a recipient of a Medical Research Council Postgraduate Research Studentship from King's College, London. Luis Araujo's present address is Hospital of the University of Pennsylvania, Philadelphia, PA, USA.

References

Altman P L and Dittmer D S 1971 *Respiration and Circulation* (Bethesda: Federation of American Societies for Experimental Biology)

Araujo L I, Lammertsma A A, Rhodes C G, McFalls E O, Iida H, Rechavia E, Galassi A, De Silva R, Jones T and Maseri A 1991 Non-invasive quantification of regional myocardial blood flow in normal volunteers and patients with coronary artery disease using oxygen-15 labeled carbon dioxide inhalation and positron emission tomography *Circulation* **83** 875-85

Bellina C R, Parodi O, Camici P, Salvadori P A, Taddei L, Fusani L, Guzzardi R, Klassen G A, L'Abbate A and Donato L 1990 Simultaneous *in vitro* and *in vivo* validation of nitrogen-13-ammonia for the assessment of regional myocardial blood flow *J. Nucl. Med.* **31** 1335-43

Bergmann S R, Fox K A A, Rand A L, McElvany K D, Welch M J, Markham J and Sobel B E 1984 Quantification of regional myocardial blood flow *in vivo* with $H_2{}^{15}O$ *Circulation* **70** 724-33

Bergman S R, Herrero P, Markham J, Weinheimer C J and Walsh M N 1989 Noninvasive quantitation of myocardial blood flow in human subjects with O-15 labeled water and positron emission tomography *J. Am. Coll. Cardiol.* **14** 639-52

Blomqvist G 1984 On the construction of functional maps in positron emission tomography *J. Cereb. Blood Flow Metab.* **4** 629-32

Budinger T F, Yano Y, Derenzo S E, Huesman R H, Yen C, Moyer B R and Sherman L G 1980 Infarction sizing and myocardial perfusion measurements using rubidium-82 and positron emission tomography *Am. J. Cardiol.* **45** 39

Crystal G J, Downey H F and Bashour H F 1981 Small vessel and total coronary blood volume during intracoronary adenosine *Am. J. Physiol.* **241** H194-H201

Eichling J O, Raichle M E, Grubb R L Jr and Ter-Pogossian M M 1974 Evidence of the limitations of water as a freely diffusible tracer in brain of the rhesus monkey *Circ. Res.* **35** 358-64

Go K G, Lammertsma A A, Paans A M J, Vaalburg W and Woldring M G 1981 Extraction of water labeled with oxygen 15 during single-capillary transit: Influence of blood pressure, osmolarity, and blood-brain barrier damage *Arch. Neurol.* **38** 581-4

Herrero P, Markham J, Shelton M E, Weinheimer C J and Bergmann S R 1990 Noninvasive quantification of regional myocardial perfusion with rubidium-82 and positron emission tomography: exploration of a mathematical model *Circulation* **82** 1377-86

Herscovitch P, Raichle M E, Kilbourn M R and Welch M J 1987 Positron emission tomographic measurement of cerebral blood flow and permeability - surface area product of water using [^{15}O] water and [^{11}C] butanol *J. Cereb. Blood Flow Metab.* **7** 527-42

Heymann M A, Payne B D, Hoffman J I E and Rudolph A M 1977 Blood flow measurements with radionuclide-labeled particles *Prog. Cardiovasc. Dis.* **20** 55-79

Hoffman E J, Huang S C and Phelps M E 1979 Quantitation in positron emission tomography: 1. effect of object size *J. Comput. Assist. Tomogr.* **3** 299-308

Huang S C, Schwaiger M, Carson R E, Carson J, Hansen H, Selin C, Hoffman E J, MacDonald N, Schelbert H R and Phelps M E 1985 Quantitative measurement of myocardial blood flow with oxygen-15 water and positron computed tomography: an assessment of potential and problems *J. Nucl. Med.* **26** 616-25

Huang S C, Williams B A, Krivokapich J, Araujo L, Phelps M E and Schelbert H R 1989 Rabbit myocardial ^{82}Rb kinetics and a compartmental model for blood flow estimation *Am. J. Physiol.* **256** H1156-H1164

Hutchins G D, Schwaiger M, Rosenspire K C, Krivokapich J, Schelbert H R and Kuhl D E 1990 Noninvasive quantification of regional blood flow in the human heart using N-13 ammonia and dynamic positron emission tomographic imaging *J. Am. Coll. Cardiol.* **15** 1032-42

ICRP 1974 *Reference Man: Anatomical, Physiological and Metabolic Characteristics* Publication 23 (Oxford : Pergamon)

Iida H, Kanno I, Takahashi A, Miura S, Murakami M, Takahashi K, Ono Y, Shishido F, Inugami A, Tomura N, Higano S, Fujita H, Sasaki H, Nakamichi H, Mizusawa S, Kondo Y and Uemura K 1988 Measurement of absolute myocardial blood flow with $H_2{}^{15}O$ and dynamic positron-emission tomography: strategy for quantification in relation to the partial-volume effect *Circulation* **78** 104-115

Iida H, Rhodes C G, Kanno I, Jones T, De Silva R and Araujo L I 1990 Noninvasive LV time-activity curve (TAC) as an input function in $H_2{}^{15}O$ dynamic PET *J. Nucl. Med.* **31** S778

Johnson J A, Cavert H M and Lifson N 1952 Kinetics concerned with distribution of isotopic water in isolated dog heart and skeletal muscle *Am. J. Physiol.* **171** 687-93

Kety S S 1951 The theory and applications of the exchange of inert gas at the lungs and tissues *Pharmacol. Rev.* **3** 1-41

——— 1960a Theory of blood-tissue exchange and its application to measurement of blood flow *Methods Med. Res.* **8** 223-7

——— 1960b Measurement of local blood flow by the exchange of an inert, diffusible substance *Methods Med. Res.* **8** 228-36

Koeppe R A, Hutchins G D, Rothley J M and Hichwa R D 1987 Examination of assumptions for local cerebral blood flow studies in PET *J. Nucl. Med.* **28** 1695-703

Krivokapich J, Smith G T, Huang S C, Hoffman E J, Ratib O, Phelps M E and Schelbert H R 1989 Nitrogen-13 ammonia myocardial imaging at rest and with exercise in normal volunteers: quantification of coronary flow with positron emission tomography *Circulation* **80** 1328-37

Lammertsma A A, Cunningham V J, Deiber M P, Heather J D, Bloomfield P M, Nutt J, Frackowiak R S J and Jones T 1990 Combination of dynamic and integral methods for generating reproducible functional CBF images *J. Cereb. Blood Flow Metab.* **10** 675-86

Lammertsma A A, Jones T, Frackowiak R S and Lenzi G L 1981 A theoretical study of the steady-state model for measuring regional cerebral blood flow and oxygen utilisation using oxygen-15 *J. Comput. Assist. Tomogr.* **5** 544-50

Martin W R W, Powers W J and Raichle M E 1987 Cerebral blood volume measured with inhaled $C^{15}O$ and positron emission tomography *J. Cereb. Blood Flow Metab.* **7** 421-6

Mullani N A, Goldstein R A, Gould K L, Marani S K, Fisher D J, O'Brien H A A Jr and Loberg M D 1983 Perfusion imaging with rubidium-82: I. measurement of extraction and flow with external detectors *J. Nucl. Med.* **24** 898-906

Paulson O B, Hertz M M, Bolwig T G and Lassen N A 1977 Filtration and diffusion of water across the blood-brain barrier in man *Microvasc. Res.* **13** 113-24

Rose C P, Goresky C A and Bach G G 1977 The capillary and sarcolemnal barriers in the heart *Circ. Res.* **41** 515-33

Schelbert H R, Phelps M E, Hoffman E J, Huang S C, Selin C E and Kuhl D E 1979 Regional myocardial perfusion assessed with N-13 labeled ammonia and positron emission computerized axial tomography *Am. J. Cardiol.* **43** 209-18

Schelbert H R, Phelps M E, Huang S C, MacDonald N S, Hansen H, Selin C and Kuhl D E 1981 N-13 ammonia as an indicator of myocardial blood flow *Circulation* **63** 1259-72

Selwyn A P, Allan R M, L'Abbate A, Horlock P, Camici P, Clark J, O'Brian H A and Grant P M 1982 Relation between regional myocardial uptake of rubidium-82 and perfusion: absolute reduction of cation uptake in ischemia *Am. J. Cardiol.* **50** 112-21

Spinks T J, Jones T, Gilardi M C and Heather J D 1988 Physical performance of the latest generation of commercial positron scanner *IEEE Trans. Nucl. Sci.* **NS-35** 721-5

Ter-Pogossian M M, Bergmann S R and Sobel B E 1982 Influence of cardiac and respiratory motion on tomographic reconstructions of the heart: implications for quantitative nuclear cardiology *J. Comput. Assist. Tomogr.* **6** 1148-58

Weinberg I N, Huang S C, Hoffman E J, Araujo L, Nienaber C, Grover-McKay M, Dahlbom M and Schelbert H R 1988 Validation of PET-acquired input function for cardiac studies with Rb-82 *J. Nucl. Med.* **29** 241-7

West J B and Dollery C T 1962 Uptake of oxygen-15-labelled CO_2 compared with carbon-11-labelled CO_2 in the lung *J. Appl. Physiol.* **17** 9-13

Yipintsoi T and Bassingthwaite J B 1970 Circulatory transport of iodoantipyrine and water in the isolated dog heart *Circ. Res.* **27** 461-7